Iranian Journal of Remote Sensing & GIS. *2026, 18 (2): 115-142* P-ISSN: ۲۰۰۸-۵۹۶۶, E-ISSN: ۲۵۸۸-۶۱۸۵

Original Article

Soil Erosion Susceptibility Mapping Using Sentinel-۱ Interferometric SAR Coherence and Machine Learning (Study Area: Khuzestan Province)

Masoud Soleimani, Najmeh Neysani Samany, Sara Attarchi, Ali Darvishi Boloorani*

Affiliation

Dep of Remote Sensing and GIS, Faculty of Geography, University of Tehran, Tehran, Iran

ABSTRACT

Soil erosion mapping is important to identify and investigate the spatial patterns of soil erosion to adopt sustainable development goals-based management strategies and soil conservation measures. The use of modern remote sensing approaches can be effective in improving soil erosion mapping. Changes in the coherence of Synthetic Aperture Radar Interferometry (InSAR) are related to surface characteristics due to soil erosion events. Accordingly, in this study, using a time series of Sentinel-۱ imagery over ۵ years (۲۰۱۵ to ۲۰۲۰) and the InSAR technique, multi-temporal coherence maps were generated for an area in Khuzestan Province. Using the Support Vector Machine (SVM) method, a machine learning-based classification scheme was developed. The ground truth soil erosion map of Khuzestan Province was used to train and validate the SVM. Subsequently, using features from Sentinel-۱ coherence, Landsat ۸-derived normalized difference vegetation index (NDVI), soil texture characteristics, and topography, soil erosion susceptibility maps were produced using different SVM kernels. The overall accuracy of the produced maps for the implemented kernels (linear, polynomial, radial basis function (RBF), and sigmoid) was ۷۲,۴۴٪, ۸۰٪, ۸۰,۴۴٪, and ۵۲٪, respectively. Consequently, the RBF kernel showed the highest performance in predicting different soil erosion susceptibility classes. Our results indicate that multi-temporal InSAR coherence can be used as a valuable data source for soil erosion mapping.

Keywords: soil erosion, interferometric synthetic aperture radar (InSAR), coherence, remote sensing, support vector machine, Sentinel-۱

* Corresponding Author: ali.darvishi@ut.ac.ir
DOI: https://doi.org/۱۰,۴۸۳۰۸/gisj.۲۰۲۶,۲۳۶۵۸۱,۱۲۲۸
Received: ۲۰۲۴,۰۸,۱۲
Accepted: ۲۰۲۶,۰۷,۱۲

Copyright: © ۲۰۲۶ by the authors. Submitted for possible open access publication under the terms and conditions of the Creative Commons Attribution (CC BY) license https://creativecommons.org/licenses/by/۴,۰/).

1. Introduction

Soil erosion generally refers to the detachment, transport, and deposition of soil particles driven by agents such as surface runoff and wind (Cerdà et al., 2017). Fertile soils are one of the most vital natural resources for sustaining human life (Amundson et al., 2015). As a natural geomorphic process, soil erosion has numerous adverse consequences, including the loss of nutrient-rich topsoil (Lal, 2003; Žížala et al., 2019) and alterations to the physical, chemical, and biological properties of soil (Lal, 2001; Darvishi Boloorani et al., 2023a). Ultimately, these impacts impose substantial socioeconomic costs on society (Senanayake et al., 2020; Darvishi Boloorani et al., 2023b, 2023c).

Owing to its diverse climatic conditions and rugged topography, Iran is considered one of the countries experiencing high rates of soil erosion. Over recent decades, factors such as rapid population growth, socioeconomic development, urban expansion, agricultural intensification, deforestation, land use/land cover (LULC) changes driven by both natural and anthropogenic processes, and overgrazing have further accelerated soil erosion across the country (Khodadadi et al., 2019; Esmali Ouri et al., 2020; Amiri & Argany, 2025). Consequently, the implementation of effective soil conservation and management strategies aimed at improving soil productivity and sustaining agricultural production—one of the primary sources of human food supply—requires a comprehensive understanding of soil erosion and its spatiotemporal patterns through the development of soil erosion maps.

Based on previous studies, approaches to soil erosion assessment can be generally classified into four main categories: (*i*) field-based plot experiments for measuring average soil loss; (*ii*) field surveys based on observable erosion indicators and the identification of erosion-driving factors; (*iii*) soil erosion modeling; and (*iv*) the integration of soil erosion models with spatial data–driven techniques (Senanayake et al., 2020). Modeling approaches can be further categorized into physically based, empirical, and conceptual models. Physically based models rely on field observations and the simulation of processes such as climatic conditions, runoff generation, infiltration, water balance, and vegetation growth. These models are fundamentally based on the physics of flow, sediment transport processes, and their interactions (Kandel et al., 2005). In contrast, empirical models simplify natural processes by establishing statistical relationships between model inputs and outputs. Their governing equations are derived from environmental observations that can be quantitatively calibrated and statistically validated. Representative empirical models include the Universal Soil Loss Equation (USLE), the Revised Universal Soil Loss Equation (RUSLE), and the Modified Universal Soil Loss Equation (MUSLE) (Alewell et al., 2019). Conceptual models generally combine elements of both

physically based and empirical approaches (Senanayake et al., 2020). Despite their widespread applications, these three categories of models are often associated with substantial limitations, including methodological complexity and high computational requirements.

Recently, a fourth category of approaches has emerged, focusing on predicting the influence of LULC change and climatic factors on soil erosion. Rather than directly estimating soil loss, these approaches model the susceptibility or potential of land to erosion based on the environmental variables associated with erosion processes. Over the past decade, a wide range of methods, including multi-criteria decision-making techniques (Arabameri et al., 2018, 2019; Domazetović et al., 2019), unsupervised classification methods (Žížala et al., 2019), and supervised machine learning algorithms (Sarkar & Mishra, 2018; Mosavi et al., 2020; Saha et al., 2020; Esmali Ouri et al., 2020; Lei et al., 2020; Arabameri et al., 2020, 2021), have been employed for soil erosion susceptibility mapping. As evidenced by the existing literature, considerable attention has recently been directed toward soil erosion susceptibility mapping, with machine learning techniques emerging as the dominant framework.

Remote sensing data have been widely used in soil erosion studies, both indirectly to derive key inputs for erosion models—such as vegetation characteristics, climatic variables, and topographic parameters—and directly to identify erosion features and different stages of soil degradation (Žížala et al., 2019). To date, remote sensing–based studies investigating the relationship between land use/land cover (LULC) dynamics and soil erosion have relied predominantly on optical imagery, with considerable emphasis placed on the development and application of both knowledge-driven and machine learning models. Among machine learning algorithms, artificial neural networks (ANNs) (Sarkar & Mishra, 2018; Mosavi et al., 2020), support vector machines (SVMs) (Bag et al., 2022), and random forest (RF) (Esmali Ouri et al., 2020) have demonstrated considerable potential for soil erosion susceptibility mapping.

Despite these advances and the growing number of studies in this field, relatively little attention has been paid to exploiting the capabilities of other remote sensing data sources, particularly those of synthetic aperture radar (SAR). Only a limited number of studies have investigated the application of SAR data in soil erosion modeling. Liu et al. (1999) were among the first to employ imagery from the ERS satellite with interferometric synthetic aperture radar (InSAR) coherence analysis to identify eroded areas in Spain. Recently, time-series Sentinel-1 data and InSAR coherence analysis have been used in Central and West Asia to detect areas susceptible to wind erosion (Sharifikia & Rabbani, 2020; Kim et

al., 2020). Overall, these studies highlight the considerable potential of InSAR data for identifying erosion-prone regions.

In the InSAR technique, phase information from two SAR images acquired over the same area at different times is used to generate an interferogram. An interferogram contains the phase differences recorded by the SAR sensor over a given time interval and is primarily used to monitor and measure surface deformation. Coherence is a standard product derived from InSAR processing and is commonly used to quantify the similarity between a pair of SAR images and to assess the quality of the resulting interferogram (Xuedong et al., 2018). The coherence values ranged from 0 to 1. Built-up areas, stable surfaces, and resistant geological formations generally exhibit high coherence values, whereas dynamically changing surfaces, such as vegetation cover and water bodies, typically show much lower coherence due to their pronounced temporal variability (Khalil, 2018; Amiri et al., 2026). In addition to these factors, soil erosion and the associated disruption of surface soil particles can contribute to coherence loss in InSAR observations. Based on this premise, it can be hypothesized that temporal variations in the coherence between SAR image pairs reflect the dynamics of surface processes and, therefore, provide valuable information for identifying areas susceptible to soil erosion (Ebrahimzadeh et al., 2023).

The primary objective of this study was to develop an integrated machine learning-based framework for soil erosion susceptibility mapping by exploiting the potential of Sentinel-1 InSAR coherence data. To this end, a time series of Sentinel-1 SAR imagery with high spatial and temporal resolution was employed. Given the complexity of soil erosion processes, optical and SAR data were integrated with soil texture characteristics and topographic variables to model the spatiotemporal surface changes associated with soil erosion and the disruption of surface soil particles.

Among machine learning algorithms, SVM has been widely adopted in recent years for remote sensing image classification and environmental mapping because of its ability to model complex nonlinear relationships, effectively handle high-dimensional datasets, and provide strong generalization performance (Maxwell et al., 2018; Huang & Zhao, 2018; Haftu et al., 2025; Boussalim & Dallahi, 2026). Compared with many conventional classification methods, SVM is also less sensitive to limited training data and, by incorporating the principle of structural risk minimization, has demonstrated a strong capability for modeling complex environmental processes, including soil erosion (Cortes & Vapnik, 1995; Mountrakis et al., 2011; Arabameri et al., 2021; Muratoreanu et al., 2025). Accordingly, the SVM classifier was employed in this study to model and map soil erosion susceptibility using InSAR coherence data in combination

with environmental variables. To implement and evaluate the proposed framework, a region within Khuzestan Province, one of the areas experiencing high annual soil erosion rates in Iran, was selected as the study area.

2. Materials and methods

As illustrated in the workflow presented in Fig. 1, the proposed methodology consists of four stages. In the first stage, InSAR processing was performed using an approximately five-year time series (from late 2015 to early 2020) of Sentinel-1 imagery with a 24-day temporal resolution to generate multi-temporal coherence map. The Small BAseline Subset (SBAS) algorithm was employed to select SAR image pairs with short spatial and temporal baselines for interferogram generation and subsequent estimation of coherence.

In the second stage, spatial datasets representing key environmental variables associated with soil erosion, including soil texture, elevation, slope, and vegetation cover, were generated and prepared. To incorporate the temporal dynamics of vegetation—one of the most influential factors affecting soil erosion—into the modeling framework, multispectral Landsat 8 imagery was processed to derive the normalized difference vegetation index (NDVI). In this study, topographic variables, vegetation cover, and soil texture were selected because of their well-established and direct roles in controlling soil erosion processes. Elevation and slope influence runoff energy, flow concentration, and sediment transport, whereas soil texture characteristics, represented by sand, silt, and clay fractions, govern soil permeability, structural stability, and susceptibility to erosion. Vegetation cover also plays a critical role in mitigating soil erosion by reducing raindrop impact, increasing surface roughness, and stabilizing soil particles. Accordingly, a time series of NDVI was incorporated into the model to account for temporal variations in vegetation cover. The selection of these environmental variables was based not only on the physical principles governing soil erosion but also on previous studies on soil erosion susceptibility modeling and mapping (Borrelli et al., 2017; Rahmati et al., 2019; Mohebzadeh et al., 2022).

After the input variables were prepared, training and validation samples were generated from the reference soil erosion map of the study area. In the fourth stage, the SVM classifier was trained using the prepared input variables and training samples with different kernel functions. Finally, a soil erosion susceptibility map was produced and validated for each kernel.

2.1. Study area

Khuzestan Province, located in southwestern Iran, is one of the country's most erosion-prone regions owing to the combined influence of its distinctive geomorphological setting, arid to semi-arid climate, diverse

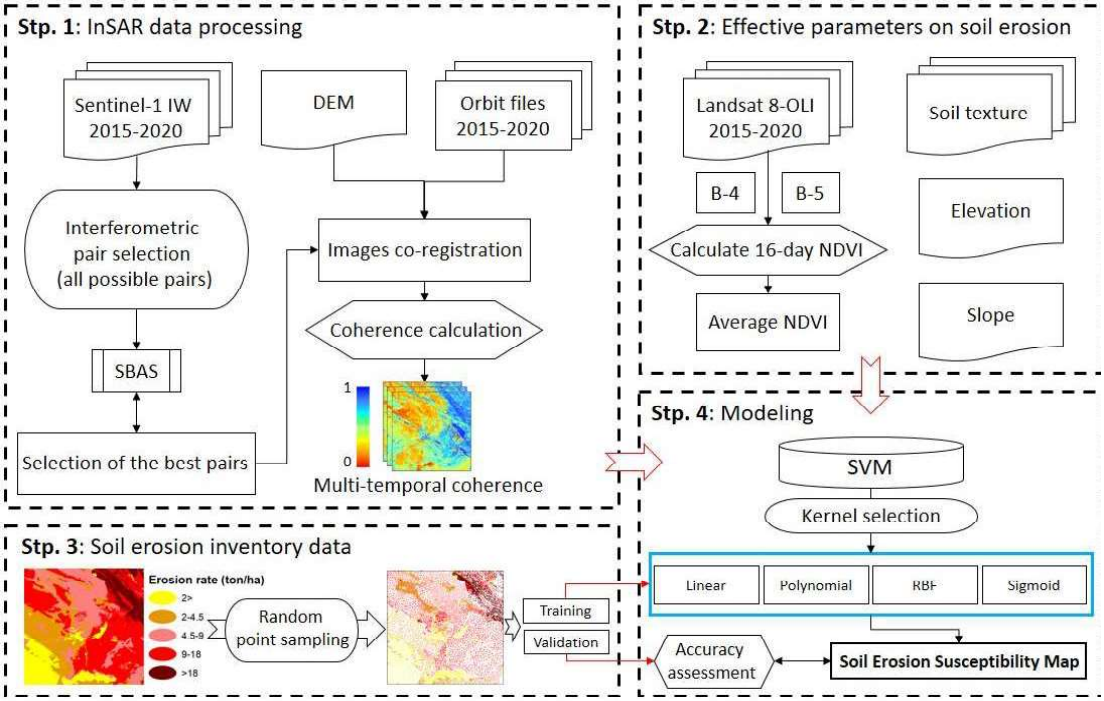


Fig. 1. Workflow of the proposed framework for InSAR coherence-based soil erosion susceptibility mapping.

geological formations, and active hydrological systems. Topographically, the northern part of the province is characterized by mountainous terrain with relatively steep slopes, where soil erosion is predominantly driven by intense rainfall events and surface runoff (Ebrahimzadeh et al., 2023). In contrast, the central and southern parts consist of extensive alluvial plains with gentle slopes that are primarily affected by wind erosion and dust activity (Bakhtiari et al., 2021). This pronounced topographic variability contributes substantially to the spatial heterogeneity of erosion processes across the province. According to the General Directorate of Natural Resources and Watershed Management of Khuzestan Province, annual soil erosion rates range from approximately 4 to 50 t ha^{-1} yr^{-1} across different parts of the province, placing Khuzestan among the regions experiencing the highest soil erosion rates in Iran (Ebrahimzadeh et al., 2023).

The study area covers part of the central plains of Khuzestan Province, extending approximately from 48°10′ to 49°20′ E and 30°45′ to 32°03′ N (Fig. 2). The area is situated within a flat alluvial plain exhibiting a diverse range of land use types, including rangelands, cultivated agricultural fields—particularly the Dehkhoda and Salman Farsi sugarcane agro-industrial companies located north and south of Ahvaz—abandoned croplands, as well as sparsely vegetated and bare soil surfaces (Soleimani et al., 2021).

From a geological perspective, young alluvial deposits are the dominant surficial units throughout the study area. These deposits comprise unconsolidated Quaternary sediments, including gravel, sand, silt, and clay, which exhibit low mechanical stability because of their weak particle cohesion and limited compaction, making them highly susceptible to erosion. Beneath these surficial deposits and along the margins of the alluvial plain, several sedimentary formations are exposed, most notably the Gachsaran Formation, which is composed primarily of marl, gypsum, and evaporitic layers, together with localized limestone and sandstone formations such as the Aghajari and Bakhtiari formations. Among these, the Gachsaran Formation is particularly vulnerable to both dissolution and mechanical erosion because of its marl-rich composition and abundant gypsum and evaporite layers, whereas limestone and sandstone units exhibit comparatively greater resistance to erosional processes. The coexistence of unconsolidated alluvial sediments at the surface and mechanically weak marl–evaporite formations in the subsurface increases the geomorphological susceptibility of the area and plays a significant role in intensifying both water- and wind-induced soil erosion (Ebrahimzadeh et al., 2023).

In addition, the presence of major perennial rivers, particularly the Karun River, together with an extensive drainage network and the occurrence of high-intensity rainfall events, provides favorable conditions for accelerated water erosion and sediment transport. Owing to its high geomorphological sensitivity and the diversity of erosion-controlling factors, the selected area represents an appropriate natural laboratory for investigating soil erosion processes. The geographical characteristics and relative and absolute location of the study area in southwestern Iran are presented in Fig. 2.

2.2. Input data

In this study, a combination of SAR imagery, optical imagery, soil texture characteristics (sand, silt, and clay content), and topographic variables (elevation and slope) were used as inputs to the SVM classifier for soil erosion susceptibility mapping.

The SAR dataset consisted of 62 Sentinel-1A C-band (wavelength ≈ 5.6 cm) interferometric wide-swath (IW) images acquired over Frame 11 (yellow rectangle in Fig. 2) with a 24-day revisit interval between November 13, 2015, and January 3, 2020. In the IW acquisition mode, data were collected over a 250-km swath width with a single-look spatial resolution of approximately 5 m in the slant-range direction and 20 m in the azimuth direction. This acquisition mode employs the Terrain Observation with Progressive Scans (TOPSAR) technique, in which the scene is imaged using three sub-swaths, designated IW1 (lowest incidence angle) to IW3 (highest incidence angle). Each sub-swath comprises multiple bursts, which are subsequently processed as individual SAR images. After

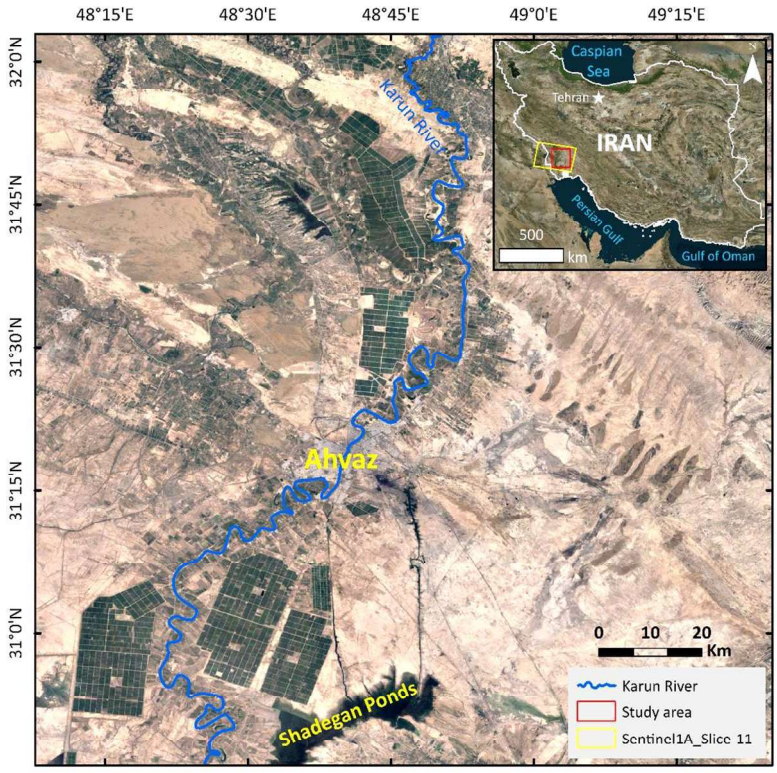


Fig. 2. Geographic location of the study area in Khuzestan Province, Iran. The background of the map is a high-resolution Google Earth image acquired in late 2020.

standard preprocessing, Sentinel-1 IW data are provided as Level-1 single-look complex (SLC) products containing both amplitude and phase information, making them suitable for InSAR applications (Soleimani et al., 2021).

The optical dataset comprised a 16-day time series of Landsat 8 Operational Land Imager (OLI) bands 4 (red) and 5 (near-infrared), with a spatial resolution of 30 m, covering the period from November 2015 to January 2020, which closely matches the temporal coverage of the SAR dataset. These data were used to derive the NDVI.

To incorporate soil texture and topographic information into the modeling framework, SoilGrids data with a spatial resolution of 250 m (Hengl et al., 2017) (Fig. 3) and the Shuttle Radar Topography Mission (SRTM) Digital Elevation Model (DEM) with a spatial resolution of 30 m (Rodriguez et al., 2006) (Fig. 4) were used.

2.3. Interferometric SAR coherence

InSAR conventionally exploits SAR images acquired over the same area from slightly different satellite positions (i.e., successive orbital passes) to generate DEM and monitor ground deformation and surface changes. In this technique, the phase difference between two co-registered SAR acquisitions is used to generate an interferogram, which represents the phase variation associated with surface

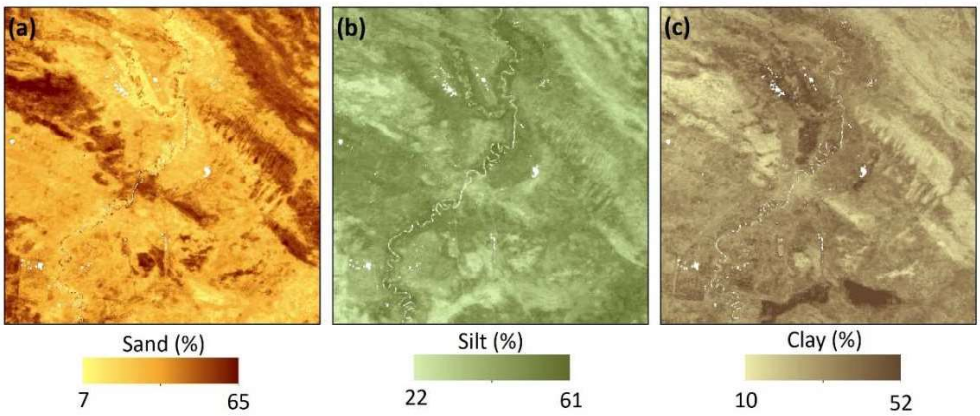


Fig. 3. Soil texture characteristics of the study area: (a) sand content, (b) silt content, and (c) clay content.

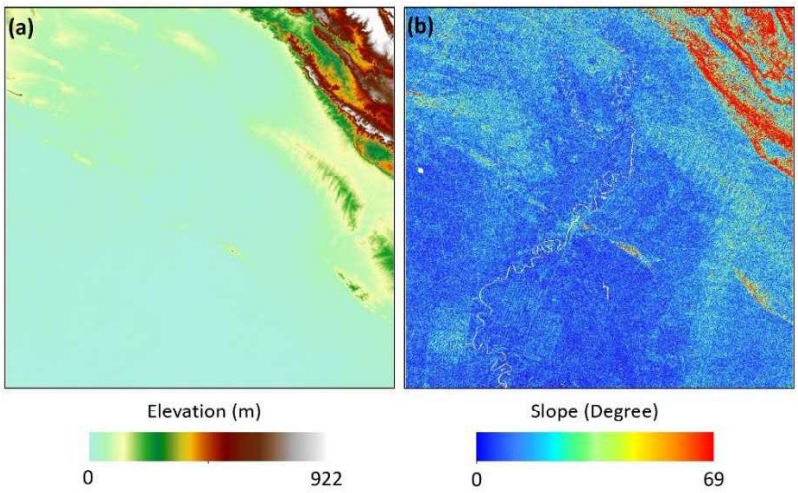


Fig. 4. Topographic datasets of the study area: (a) elevation above mean sea level and (b) slope derived from the DEM.

changes occurring between the two acquisition dates (Hanssen, 2002; Simons & Rosen, 2007). One of the main products derived from InSAR processing is the coherence image, which is commonly used to evaluate the quality of the generated interferogram and is calculated using Eq. (1):

$$\hat{\gamma} = \frac{E\{S_1 S_2^*\}}{\sqrt{E\{S_1 S_1^*\}.E\{S_2 S_2^*\}}} \qquad \text{Eq.(1)}$$

where E {0} denotes the expectation operator, and S_1 and S_2 represent two co-registered complex SAR images. In practical applications, assuming that S_1 and S_2 are stochastic signals, the expectation operator is approximated by the spatial average of pixels within a moving window (Touzi et al., 1999). Accordingly, Eq. (1) can be rewritten as Eq. (2):

$$\gamma = \frac{\frac{1}{L}\sum_{l=1}^{L} S_1 S_2^*}{\sqrt{\frac{1}{L}(\sum_{l=1}^{L} S_1 S_1^*).\frac{1}{L}(\sum_{l=1}^{L} S_2 S_2^*)}} \qquad (L>1)$$

Eq.(2)

where L denotes the number of samples within the moving window. The coherence coefficient (γ) ranges from 0 to 1, where lower values indicate weak coherence and higher values indicate strong coherence. Coherence behavior varies considerably across different LULC types. Urban areas and other stable man-made surfaces generally exhibit consistently high coherence because of their limited temporal variability. In contrast, vegetated areas typically experience substantial coherence loss owing to phenological changes and vegetation dynamics over time (Soleimani et al., 2021). Soil erosion processes induced by water or wind involve the detachment, displacement, and redistribution of surface soil particles, which alter the physical characteristics of the ground surface. These surface modifications reduce the similarity between successive SAR acquisitions and consequently lead to coherence loss. Therefore, the temporal analysis of InSAR coherence provides valuable information for characterizing and mapping soil erosion processes (Ebrahimzadeh et al., 2023).

Several error sources in InSAR processing may obscure the surface-change signal contained in the SAR phase observations and consequently introduce noise into coherence measurements, thereby reducing their effectiveness for soil erosion modeling. Among these, spatial and temporal decorrelation are two of the most common sources of coherence degradation. Spatial decorrelation arises from differences in imaging geometry between the master and slave acquisitions, whereas temporal decorrelation results from changes in surface properties and atmospheric conditions between acquisition dates. These effects frequently produce interferograms containing extensive areas of low coherence (Papi et al., 2020). The SBAS algorithm is one of the most widely adopted approaches for mitigating spatial and temporal decorrelation. In this method, interferograms are generated only from image pairs characterized by short spatial baselines (typically <200 m) and short temporal baselines, thereby improving coherence and reducing decorrelation effects (Berardino et al., 2003).

Because SAR images acquired at different times are not perfectly aligned geometrically, accurate co-registration to a common reference image is essential before coherence analysis. This step ensures pixel-level correspondence among all acquisitions and enables a reliable assessment of temporal surface changes. Accordingly, as illustrated in Fig. 1, all SAR images were first co-registered to a common reference geometry using precise orbit information, together with a DEM covering the study area. From the 62 SAR acquisitions, a total of 1,891 possible image pairs were initially considered according to the combination rule $\binom{n}{2}$. Applying the SBAS selection criteria yielded 95 interferometric pairs with spatial baselines shorter than 200 m and temporal baselines not

exceeding 72 days. The corresponding multi-temporal coherence images were subsequently generated using Eq. (2).

Because coherence reduction in InSAR may result from a combination of factors, including geometric inaccuracies, image misregistration, atmospheric effects (particularly tropospheric water vapor delays), and genuine surface changes, a series of standard processing strategies was implemented to minimize these error sources and increase confidence that the observed coherence variations primarily reflect physical changes at the land surface. Specifically, the SBAS framework, together with short spatial (<200 m) and temporal (≤72 days) baseline thresholds, substantially reduced geometric and temporal decorrelation by retaining only highly coherent interferometric pairs. Furthermore, precise co-registration based on orbit information and the DEM minimized image misregistration errors. Coherence was also estimated using spatial averaging within a moving window, following the standard InSAR approach, which effectively suppresses speckle noise and improves the statistical stability of the coherence estimates.

Interferogram and coherence generation were performed using the GMTSAR software package, which incorporates adaptive spectral filtering techniques, including the Goldstein filter. These filters are primarily designed to improve phase quality and suppress speckle noise rather than explicitly model or remove atmospheric delays, such as tropospheric effects. Nevertheless, the multi-temporal SBAS framework inherently reduces the influence of atmospheric noise because these effects are largely random over time and are therefore attenuated during temporal integration. Although complete elimination of all InSAR error sources is not feasible, the combination of these processing strategies substantially improves the reliability of the coherence time series, allowing the majority of the observed coherence variations to be attributed with greater confidence to actual physical changes occurring at the Earth's surface.

2.4. Reference soil erosion data

Training the SVM classifier for soil erosion susceptibility mapping requires reliable reference data that represent different levels of soil erosion within the study area. For this purpose, the official soil erosion map of Khuzestan Province, produced by the Forests, Rangelands, and Watershed Management Organization of Iran (FRWMO) based on field surveys and empirical erosion models, was used as the reference dataset. The annual soil erosion rate was classified into five categories. Assuming that areas with higher erosion rates are more susceptible to future soil erosion than areas with lower erosion rates, these five erosion rate classes were directly considered the five soil erosion susceptibility classes used in this study. Subsequently, a stratified random

sampling strategy was employed to generate the training and validation samples, with an average of approximately 250 sample points selected for each susceptibility class, while ensuring an appropriate spatial distribution across the study area (Fig. 5).

2.5. Support Vector Machine (SVM) classifier

The SVM, developed within the framework of statistical learning theory, has been widely adopted as a powerful machine learning algorithm for solving complex classification and regression problems. Originally designed as a supervised binary classifier, SVM seeks to identify the optimal separating hyperplane that maximizes the margin between two classes (Vapnik, 2013). The training samples located closest to the decision boundary, which defines the optimal margin, are referred to as support vectors (Kavzoglu et al., 2014).

In many remote sensing applications, the input data are not linearly separable. To address this limitation, SVM employs kernel functions to map the original data into a higher-dimensional feature space, where linear separation can be achieved more

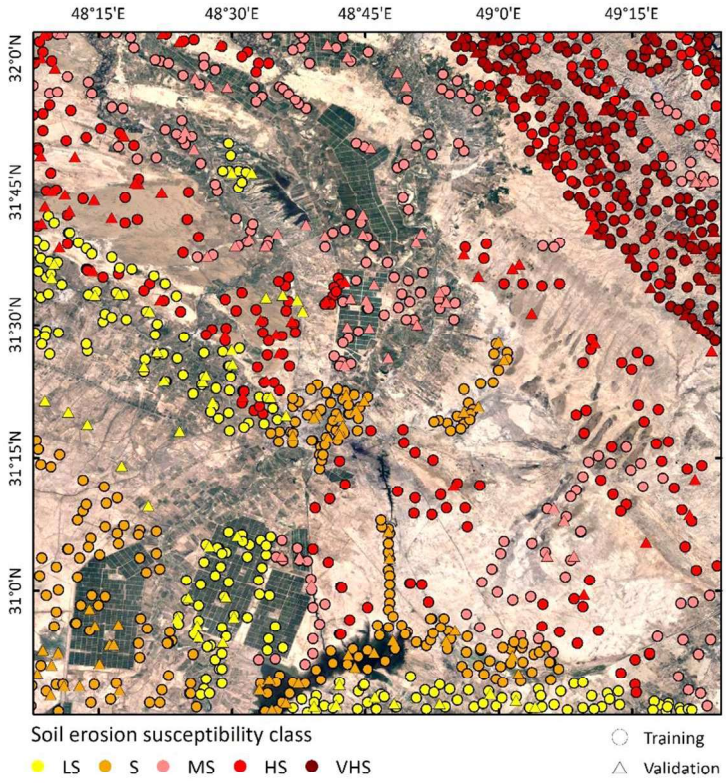


Fig. 5. Training and validation samples were randomly selected from the reference soil erosion map of the study area for SVM model development. A total of 200, 224, 200, 217, and 200 randomly distributed points were selected for the very high susceptibility (VHS), high susceptibility (HS), moderate susceptibility (MS), susceptible (S), and low susceptibility (LS) classes, respectively, as training samples (colored circles). In addition, 45 independent validation points were randomly selected for each class (colored triangles).

effectively (Cortes & Vapnik, 1995; Ren et al., 2018). This capability enables SVM to model complex nonlinear relationships while maintaining robust and reliable performance (Pal & Mather, 2005; Mountrakis et al., 2011).

In this study, four widely used kernel functions—linear, polynomial, radial basis function (RBF), and sigmoid—were evaluated to model both linear and nonlinear relationships between the input variables and soil erosion susceptibility classes. To optimize model performance, the parameters of each kernel were systematically tuned. Because simultaneously optimizing all kernel parameters would substantially expand the search space and increase the computational cost, only the most influential parameters governing model performance were selected for optimization. This strategy maintained computational efficiency while avoiding unnecessary model complexity. Accordingly, the penalty parameter (C) and Gaussian kernel width (γ) were optimized for all kernels. The parameter C controls the trade-off between model complexity and classification error, whereas γ determines the influence of individual training samples and the flexibility of the decision boundary (Smola & Schölkopf, 2004; Goel & Srivastava, 2016). For the linear kernel, only C was optimized, whereas the polynomial degree (degree) was additionally tuned for the polynomial kernel.

The optimal parameter values were determined using a grid search combined with five-fold cross-validation. The search space was defined on a logarithmic scale spanning several orders of magnitude, allowing comprehensive exploration of candidate parameter values while reducing bias associated with parameter selection (Arlot & Celisse, 2010; Syarif et al., 2016). Specifically, parameter C was evaluated over the values 0.1, 1, 10, 100, and 1000. The γ parameter was tested at 0.001, 0.01, 0.1, and 1, while the polynomial kernel degree was evaluated for 2, 3, 4, and 5. The final kernel and its corresponding optimal parameter values were selected based on the highest classification performance achieved during the cross-validation procedure.

2.6. Accuracy assessment

Accuracy assessment is an essential step in evaluating the reliability of the thematic maps. One of the most widely adopted approaches for assessing the performance of classification models is the confusion matrix, which compares the predicted class labels with the corresponding reference labels. In a confusion matrix, correctly classified samples are located along the main diagonal, whereas off-diagonal elements represent classification errors.

Among the evaluation metrics derived from the confusion matrix, OA is the most commonly reported indicator, expressing the proportion of correctly classified samples relative to the total number of validation samples. Another widely used metric is the

Kappa coefficient (KC), which provides a more robust measure of classification agreement by accounting for the agreement expected by chance. Compared with OA, KC offers a more comprehensive evaluation because it considers both correctly and incorrectly classified samples. In addition, User's Accuracy (UA) and Producer's Accuracy (PA) were calculated for each erosion susceptibility class to quantify class-specific classification performance (Jensen, 1996).

Accordingly, as illustrated in Fig. 5, 225 independent reference samples (45 samples for each erosion susceptibility class) were used to validate the generated soil erosion susceptibility maps. The final accuracy assessment was performed by constructing confusion matrices and calculating OA, KC, UA, and PA.

3. Results and discussion

3.1. Analysis of InSAR coherence

A total of 95 coherence images corresponding to different temporal intervals were generated over the study area using the InSAR processing workflow. The annual mean coherence maps are presented in Fig. 6, which clearly illustrates the spatial and temporal variability of coherence throughout the study period. Because only interferometric pairs with high coherence and, consequently, short temporal and perpendicular baselines were selected, the effects of temporal decorrelation associated with atmospheric variations and spatial decorrelation caused by orbital separation were minimized as much as possible. Therefore, the observed coherence patterns are expected to primarily reflect actual changes in the physical characteristics of the land surface. As shown in Fig. 6, areas displayed in blue generally exhibit high coherence values, indicating relatively stable surface conditions throughout the observation period. In contrast, the red-colored areas are characterized by substantially lower coherence values, reflecting pronounced changes in the surface backscattering properties over time.

The fundamental assumption underlying InSAR coherence-based soil erosion modeling is that soil erosion processes, through the detachment and displacement of surface soil particles, reduce the temporal coherence of SAR image pairs. However, soil erosion is not the only process that can cause coherence loss. Highly dynamic LULC types, particularly water bodies and vegetation cover, exhibit low coherence because of their rapid temporal variability (Amiri et al., 2026). Consequently, although multi-temporal coherence provides valuable information on surface dynamics, it cannot independently distinguish erosion-induced changes from other sources of temporal decorrelation. This limitation highlights the necessity of incorporating additional environmental variables that are known to influence soil erosion. Accordingly, in addition to InSAR coherence, the present study integrated key environmental drivers,

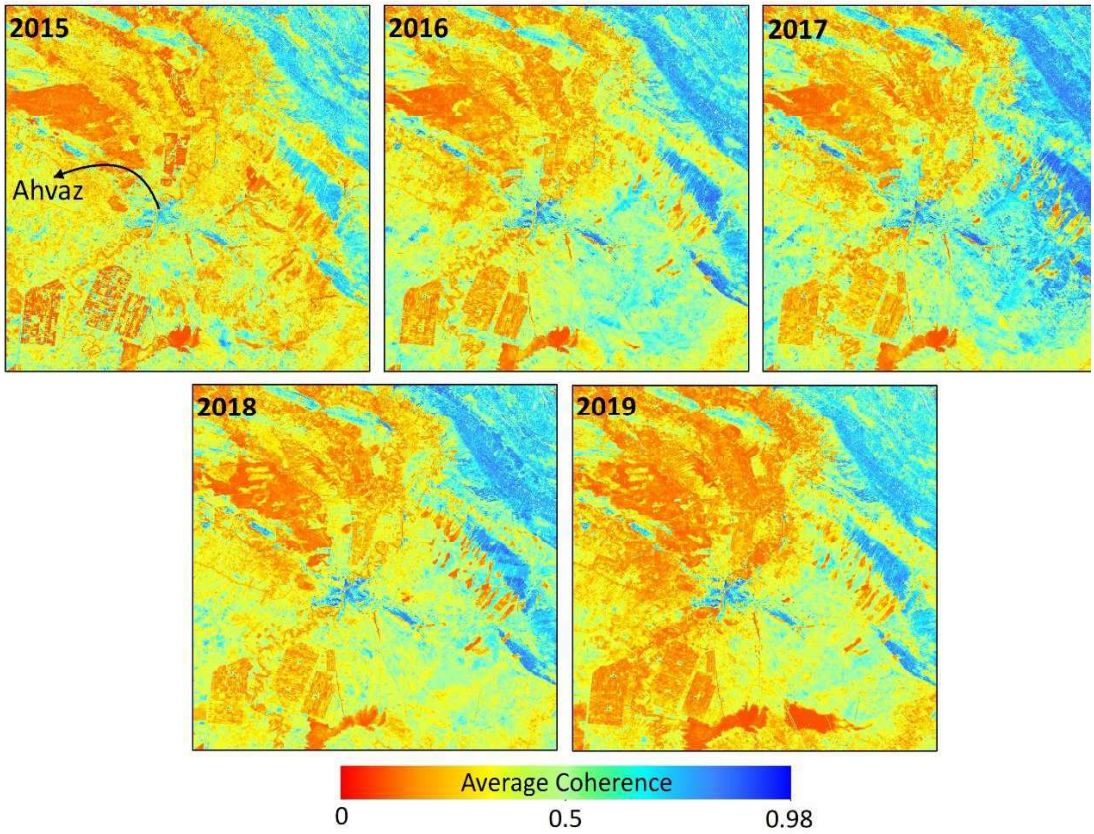


Fig. 6. Annual mean InSAR coherence maps were derived from the processing of the Sentinel-1 time-series dataset.

including vegetation dynamics, soil texture characteristics, and topographic factors, into the modeling framework.

Fig. 7 presents the monthly mean NDVI maps for the period from 2015 to 2020 over the study area. The generated maps reveal the spatial distribution of vegetation through a range of blue color tones. Natural vegetation exhibits relatively limited temporal variation compared to managed vegetation, particularly agricultural lands. Accordingly, the sugarcane agro-industrial complexes located north and south of Ahvaz show substantially greater seasonal variability than other vegetated areas within the study region. In contrast, water bodies and moist soils are represented by brown to yellow color tones.

To capture seasonal vegetation dynamics, the monthly NDVI time series was incorporated into the SVM classifier as 12 input layers, along with the remaining environmental variables. As discussed previously, vegetated areas and water bodies exhibit considerable temporal variability, which is reflected by the high variance and reduced coherence in InSAR observations. However, pronounced temporal changes in coherence do not necessarily indicate severe soil erosion. Integrating the NDVI time series into the classification framework enabled the

model to distinguish vegetation-induced coherence variations from those associated with soil erosion processes.

It should be noted that the objective of incorporating the NDVI time series in this study was to use it as an auxiliary predictor for separating the effects of surface cover—particularly vegetation, water bodies, and agricultural land—from the InSAR coherence signal. Rather than being employed to mask or exclude specific LULC types, NDVI was introduced as one of the input features to the SVM classifier alongside other environmental variables. This enabled the algorithm to

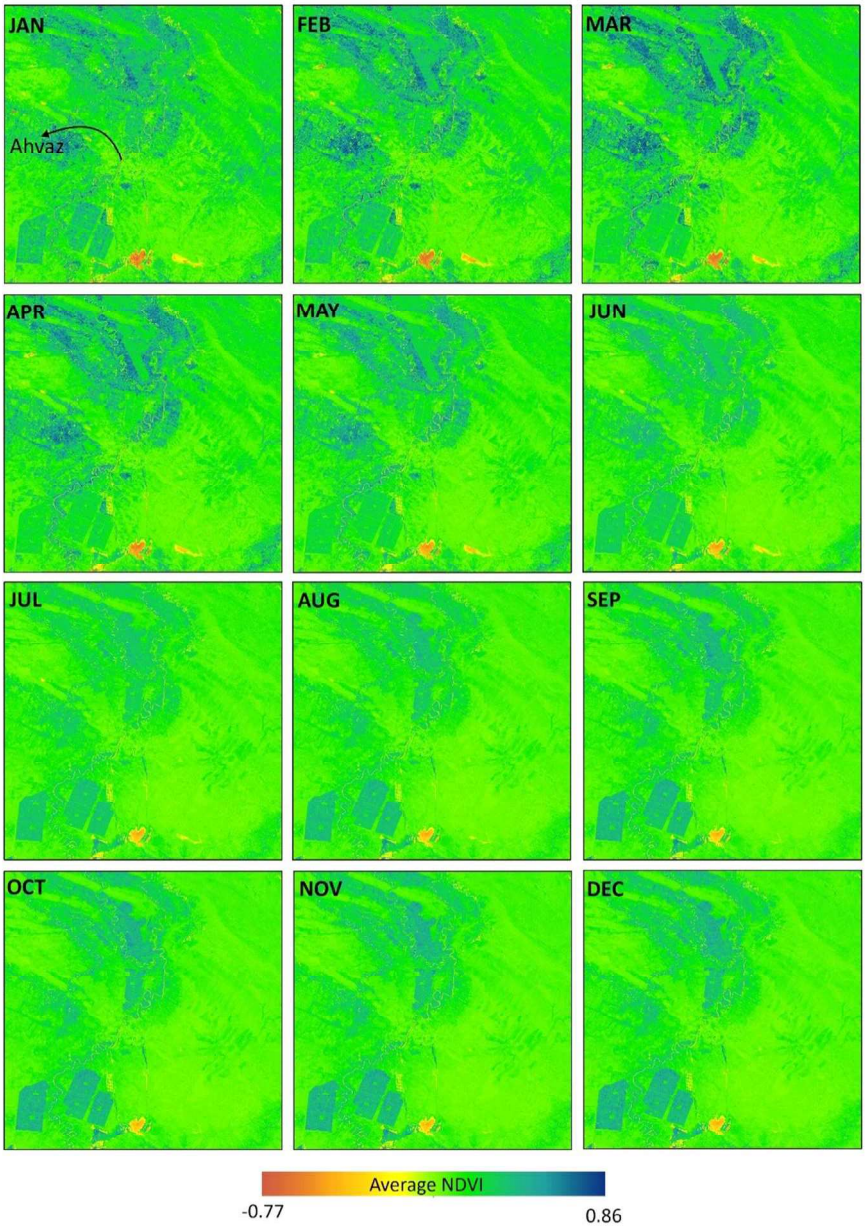


Fig. 7. Monthly mean NDVI derived from the Landsat 8 OLI multispectral time series for the 2015–2020 study period.

distinguish coherence variations caused by dynamic non-soil surface covers from patterns associated with geomorphological processes and soil erosion. In this context, NDVI serves as a controlling variable within the data-driven modeling framework, improving the model's ability to account for seasonal variability and LULC heterogeneity without requiring any manual masking or rule-based exclusion of specific areas.

3.2. Soil erosion susceptibility mapping

For SVM implementation, 112 input features were used, including 95 InSAR coherence images, 12 monthly mean NDVI images, three soil texture variables, and two topographic variables. The generated training samples were used to train the SVM classifier to identify the optimal decision hyperplane for discriminating among the predefined soil erosion susceptibility classes. During the training process, the relationships between the 112-dimensional feature space and susceptibility classes were modeled using four kernel functions—linear, polynomial, RBF, and sigmoid. For each kernel, the optimal parameter combination was determined through grid search coupled with cross-validation, and the corresponding optimized hyperplane was fitted to the training data. The optimized models were subsequently used to generate soil erosion susceptibility maps for each kernel (Fig. 8).

As illustrated in Fig. 8, the different kernel functions produced noticeably different spatial patterns of predicted soil erosion susceptibility. These differences reflect the varying capabilities of the kernels in capturing the underlying relationships in the multidimensional feature space. In particular, the distinct susceptibility patterns highlight the influence of kernel selection on modeling the complexity and nonlinearity of the input variables, leading to different representations of erosion susceptibility across the study area.

3.3. Validation of the soil erosion susceptibility maps

To evaluate the accuracy of the soil erosion susceptibility maps generated using the optimized SVM kernels (Fig. 8), the OA, KC, UA, and PA metrics were calculated based on the confusion matrix. The confusion matrices, constructed using independent validation samples and their corresponding predicted classes in the generated susceptibility maps, are presented in Tables 1–4.

The accuracy assessment results demonstrated that the RBF kernel (Table 3) outperformed the other kernels in discriminating and mapping the different soil erosion susceptibility classes. In contrast, the sigmoid kernel exhibited the lowest classification performance. The approximately 28% difference in overall accuracy between the RBF and sigmoid kernels highlights the substantial influence of kernel selection on the performance of the InSAR coherence-based soil erosion susceptibility mapping. A summary of the

confusion matrix results, including the overall accuracy and Kappa coefficient, is presented in Fig. 9 to facilitate comparison of the overall performance of the different kernel functions.

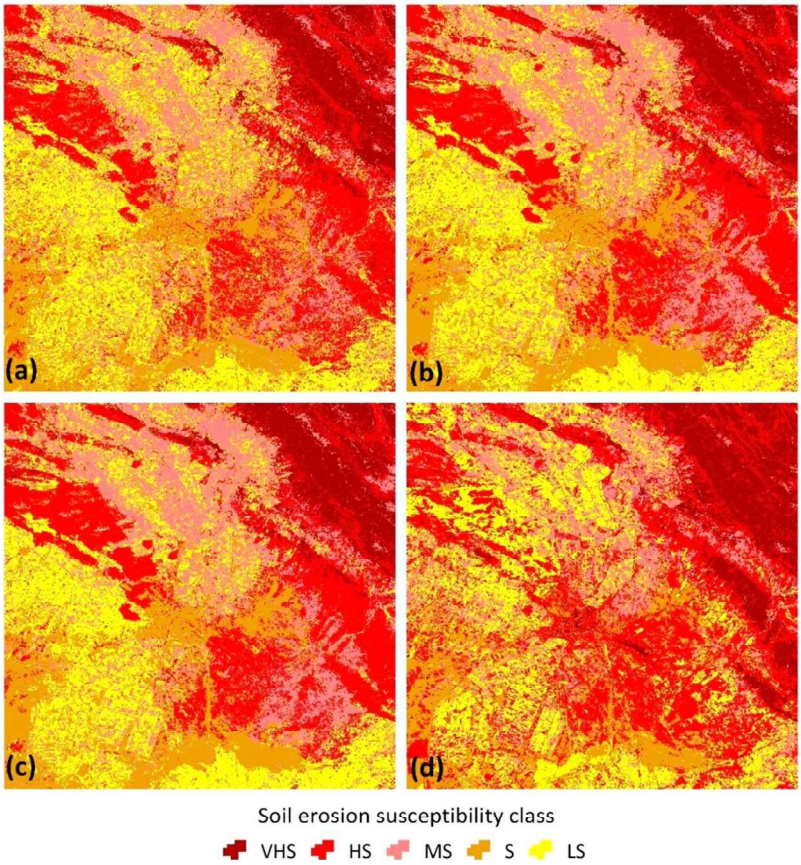


Fig. 8. Soil erosion susceptibility maps generated using different SVM kernels: (a) linear kernel, (b) second-degree polynomial kernel, (c) RBF kernel, and (d) sigmoid kernel.

Table 1. Confusion matrix for the accuracy assessment of the soil erosion susceptibility map generated using the optimized linear kernel

Error matrix		Ground reference classes (pixel)					Accuracy assessment			
		VHS	HS	MS	S	LS	UA (%)	PA (%)	OA (%)	KC (%)
Predicted classes (pixel)	VHS	39	5	0	0	0	88.64	86.67		
	HS	5	36	3	3	3	72.00	80.00		
	MS	1	2	32	3	9	68.09	71.11	72.44	65.56
	S	0	0	3	32	9	72.73	71.11		
	LS	0	2	7	7	24	60.00	53.33		

VHS: Very High Susceptible; HS: High Susceptible; MS: Moderate Susceptible; S: Susceptible; LS: Low Susceptible; UA: User Accuracy; PA: Producer Accuracy; OA: Overall Accuracy; KC: Kappa Coefficient.

Table 2. Confusion matrix for the accuracy assessment of the soil erosion susceptibility map generated using the optimized second-degree polynomial kernel.

Error matrix		Ground reference classes (pixel)					Accuracy assessment			
		VHS	HS	MS	S	LS	UA (%)	PA (%)	OA (%)	KC (%)
Predicted classes (pixel)	VHS	40	5	0	0	0	88.89	88.89		
	HS	5	36	1	2	1	80.00	80.00		
	MS	0	3	36	3	8	72.00	80.00		
	S	0	0	1	37	5	86.05	82.22	80.00	75.00
	LS	0	1	7	3	31	73.81	68.89		

Table 3. Confusion matrix for the accuracy assessment of the soil erosion susceptibility map generated using the optimized RBF kernel.

Error matrix		Ground reference classes (pixel)					Accuracy assessment			
		VHS	HS	MS	S	LS	UA (%)	PA (%)	OA (%)	KC (%)
Predicted classes (pixel)	VHS	40	5	0	0	0	88.89	88.89		
	HS	5	35	1	2	1	79.55	77.78		
	MS	0	3	36	3	7	73.47	80.00		
	S	0	1	2	37	4	84.09	82.22	80.44	75.56
	LS	0	1	6	3	33	76.74	73.33		

Table 4. Confusion matrix for the accuracy assessment of the soil erosion susceptibility map generated using the optimized sigmoid kernel.

Error matrix		Ground reference classes (pixel)					Accuracy assessment			
		VHS	HS	MS	S	LS	UA (%)	PA (%)	OA (%)	KC (%)
Predicted classes (pixel)	VHS	40	8	3	2	0	75.47	88.89		
	HS	5	18	6	18	9	32.14	40.00		
	MS	0	2	19	0	8	65.52	42.22		
	S	0	1	2	18	6	66.67	40.00	52.00	40.00
	LS	0	16	15	7	22	36.67	48.89		

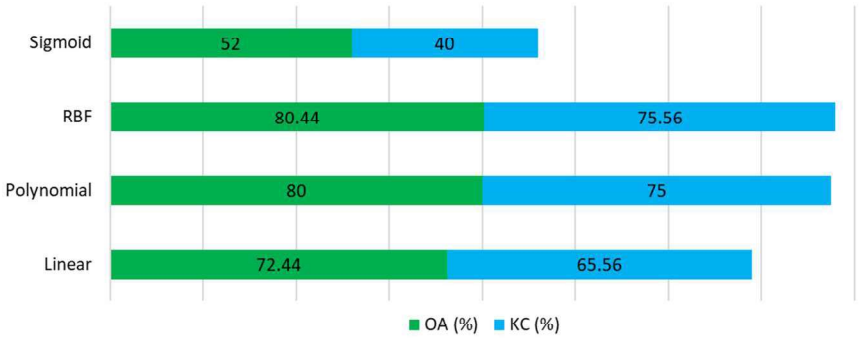


Fig. 9. The overall performance of the different SVM kernels for soil erosion susceptibility mapping was evaluated using the overall accuracy (OA) and Kappa coefficient (KC).

3.4. Analysis of the role of environmental factors in soil erosion susceptibility patterns

A spatial overlay analysis between the soil erosion susceptibility map produced by the optimized RBF kernel (Fig. 8c) and the environmental variables indicates that the predicted susceptibility patterns are closely associated with soil texture (Fig. 3) and topographic characteristics (Fig. 4).

From a pedological perspective, the results show that a substantial proportion of the high (HS) and very high (VHS) susceptibility classes coincide with areas characterized by relatively higher sand content, whereas areas with higher silt and clay contents are predominantly associated with the low-to moderate-susceptibility classes. This pattern reflects the dual role of soil texture in controlling the erosion processes. Under certain conditions, an increase in sand content can reduce interparticle cohesion and enhance the mobility of surface particles, thereby increasing erosion susceptibility. In contrast, relatively high proportions of silt and clay promote greater structural cohesion and particle retention, which can reduce the relative susceptibility to erosion at the regional scale.

From a topographic perspective, the high-susceptibility classes were primarily concentrated in areas with moderate to relatively steep slopes, confirming the critical role of slope in increasing runoff energy and intensifying soil particle detachment and transport. Conversely, areas with gentle slopes were largely classified within the low susceptibility classes (LS and S) (Fig. 8c), indicating their relatively greater stability against both water- and wind-induced erosion. The spatial distribution of the susceptibility classes further suggests that elevation alone does not exhibit a direct linear relationship with erosion susceptibility; instead, its influence is expressed mainly through its control on local slope gradients and geomorphological conditions. Overall, the close agreement between the model outputs and these independent physical variables demonstrates that the RBF-optimized SVM model, which integrates InSAR coherence data with environmental parameters, not only achieved strong statistical performance but also successfully captured the well-established physical controls governing soil erosion processes, thereby strengthening the credibility of the results.

The findings of this study are consistent with previous investigations conducted in the study area, which likewise identified topographic factors—particularly slope—as key controls on the intensity and spatial distribution of soil erosion (Ebrahimzadeh et al., 2023). Similarly, the observed pattern regarding the influence of soil texture indicates that erosion susceptibility depends not only on the relative proportions of sand, silt, and clay, but also on the interaction of these properties with hydrological conditions and topographic gradients. This behavior is

consistent with previous studies reporting that the influence of soil texture on erosion is nonlinear and strongly conditioned by the surrounding environment.

3.5. Limitations and future research

Although the results of this study demonstrate the effectiveness of integrating multi-temporal InSAR coherence with optical and environmental variables for soil erosion susceptibility mapping, several methodological limitations should be acknowledged, as they may influence the interpretation of the results of this study. One of the primary limitations is the absence of direct hydrological and climatic variables, particularly precipitation and rainfall erosivity indices (R factor). In classical soil erosion models, such as the USLE and RUSLE, rainfall erosivity is recognized as one of the principal factors controlling soil erosion rates (Panagos et al., 2015; Alewell et al., 2019). However, the exclusion of these variables from the proposed framework primarily reflects the data-driven nature and methodological objective of this study, which was to evaluate the capability of InSAR coherence data to discriminate dynamic surface changes associated with soil erosion. Accordingly, rather than attempting to explicitly reproduce the physical processes governing erosion, the proposed framework was designed to identify learnable statistical and spatiotemporal patterns from multisource datasets. Furthermore, part of the hydrological and climatic influence is indirectly reflected in the temporal dynamics of vegetation (NDVI) and the variability of InSAR coherence, as both variables are sensitive to changes in surface moisture, seasonal conditions and land surface dynamics.

From a data perspective, another major challenge was the lack of rainfall datasets with spatial and temporal resolutions consistent with those of the Sentinel-1 and Landsat-8 observations. In recent years, climate reanalysis products, such as ERA5 (Hersbach et al., 2020) and satellite-based precipitation datasets, such as CHIRPS (Funk et al., 2015), have become widely used sources for deriving precipitation variables. Nevertheless, integrating these datasets with InSAR and optical remote sensing observations requires extensive preprocessing, including spatial downscaling and temporal alignment, which was beyond the scope of the present study.

Despite these limitations, the results indicate that integrating InSAR coherence with topographic variables, soil texture characteristics, and vegetation indices can successfully capture meaningful spatial patterns of soil erosion susceptibility in the study area. These findings are consistent with recent studies highlighting the value of multi-source datasets for improving machine learning models in soil erosion assessment (Arabameri et al., 2020; Borrelli et al., 2020).

Future research should explore hybrid frameworks that combine process-based

models such as the RUSLE with data-driven approaches. In particular, incorporating rainfall erosivity factors derived from ERA5 or CHIRPS, alongside machine learning algorithms and InSAR observations, has the potential to improve the accuracy, generalizability, and interpretability of soil erosion susceptibility models. Furthermore, integrating physically based models with artificial intelligence techniques may represent an important step toward reducing uncertainty in soil erosion modeling at both regional and global scales.

In addition, this study relied exclusively on InSAR coherence as the radar-derived input feature, whereas SAR imagery provides access to a broader range of advanced information products. Future studies could incorporate SAR polarimetric features and target decomposition parameters to provide complementary information on the physical and structural characteristics of the land surface. Owing to their sensitivity to the scattering behavior of surface targets under different polarization states, these features may improve the discrimination of LULC types, facilitate the detection of structural changes in the soil surface, and enhance soil erosion modeling. Consequently, integrating SAR polarimetric features with InSAR coherence and other environmental variables may further improve both the predictive performance and interpretability of soil erosion models in future research.

4. Conclusion

This study evaluated the potential of Sentinel-1 interferometric synthetic aperture radar (InSAR) coherence data for soil erosion susceptibility mapping through an integrated machine learning framework. To this end, a five-year SAR time series was processed to generate multi-temporal InSAR coherence maps, which were subsequently combined with the normalized difference vegetation index (NDVI), soil texture characteristics, and topographic variables as input features for a support vector machine (SVM) classifier. The results demonstrated that the spatiotemporal variability of InSAR coherence provides valuable information on land surface dynamics and areas susceptible to soil erosion, particularly where structural changes and the displacement of surface soil particles lead to a progressive loss of coherence over time.

The findings further indicate that relying solely on InSAR coherence may introduce ambiguity in the interpretation of erosion patterns because coherence is highly sensitive to vegetation dynamics, surface moisture, and water bodies. Integrating InSAR coherence with multi-temporal NDVI and environmental variables effectively distinguished erosion-related changes from other sources of land-surface dynamics, thereby improving the overall performance of the model. Collectively, the integration of InSAR coherence, optical data, and environmental variables established a robust framework for modeling soil erosion susceptibility.

The performance evaluation of different SVM kernels revealed that kernel selection substantially influences the accuracy of soil erosion susceptibility mapping. Among the evaluated kernels, the radial basis function (RBF) achieved the highest performance, with an overall accuracy of 80.44% and a Kappa coefficient of 75.56%, whereas the sigmoid kernel yielded the lowest classification accuracy. These results highlight the superior capability of the RBF kernel in modeling the complex nonlinear relationships among the multisource datasets employed in this study.

Overall, the findings underscore the considerable potential of InSAR coherence for soil erosion studies and demonstrate that it can serve as a valuable complementary source of information alongside conventional remote sensing data and environmental variables. The proposed framework is particularly suitable for arid and semi-arid environments, where field-based monitoring of soil erosion is often constrained by logistical, temporal, and economic limitations; therefore, it offers a practical tool for land monitoring and management.

Although the proposed framework produced encouraging results, this study primarily focused on evaluating the capabilities of InSAR coherence and data-driven machine learning approaches for soil erosion susceptibility mapping. Future research should incorporate climatic and hydrological variables, such as precipitation, runoff, and rainfall erosivity, within hybrid frameworks that combine process-based models with artificial intelligence techniques. In addition, integrating climate reanalysis datasets, satellite-derived precipitation products, and SAR polarimetric information with multi-temporal InSAR coherence has the potential to further enhance the accuracy, generalizability, and interpretability of soil erosion models across regional and broader spatial scales.

5. References

Alewell, C., Borrelli, P., Meusburger, K. and Panagos, P., 2019. Using the USLE: Chances, challenges and limitations of soil erosion modelling. International soil and water conservation research, 7(3), pp.203-225. https://doi.org/10.1016/j.iswcr.2019.05.004

Amiri, F., Argany, M., 2025. Assessment and forecasting of surface water changes in the Hamoun Lakes using Landsat imagery and CA-Markov model. Iranian Journal of Remote Sensing and GIS, (), pp. -. https://doi.org/10.48308/gisj.2025.235084.1211 (Persian).

Amiri, F., Shamsoddini, A. and Sharifikia, M., 2026. Evaluating the Efficiency of InSAR Coherence in Crop Type Mapping Using Machine Learning. Iranian Journal of Remote Sensing and GIS. 17(4), pp.133-160. https://doi.org/10.48308/gisj.2025.238522. 1249 (Persian).

Amundson, R., Berhe, A.A., Hopmans, J.W., Olson, C., Sztein, A.E. and Sparks, D.L., 2015. Soil and human security in the 21st century. Science, 348(6235), p.1261071. https://doi.org/10.1126/science.1261071

Arabameri, A., Chandra Pal, S., Costache, R., Saha, A., Rezaie, F., Seyed Danesh, A., Pradhan, B., Lee, S. and Hoang, N.D., 2021. Prediction of gully erosion susceptibility mapping using novel ensemble machine learning algorithms. Geomatics, Natural Hazards and Risk, 12(1), pp.469-498. https://doi.org/10.1080/19475705.2021.1880977

Arabameri, A., Chen, W., Loche, M., Zhao, X., Li, Y., Lombardo, L., Cerda, A., Pradhan, B. and Bui, D.T., 2020. Comparison of machine learning models for gully erosion susceptibility mapping. Geoscience Frontiers, 11(5), pp.1609-1620. https://doi.org/10.1016/j.gsf.2019.11.009

Arabameri, A., Pradhan, B., Pourghasemi, H.R. and Rezaei, K., 2018. Identification of erosion-prone areas using different multi-criteria decision-making techniques and GIS. Geomatics, Natural Hazards and Risk, 9(1), pp.1129-1155. https://doi.org/10.1080/19475705.2018.1513084

Arabameri, A., Pradhan, B., Rezaei, K. and Conoscenti, C., 2019. Gully erosion susceptibility mapping using GIS-based multi-criteria decision analysis techniques. Catena, 180, pp.282-297. https://doi.org/10.1016/j.catena.2019.04.032

Arlot, S. and Celisse, A., 2010. A survey of cross-validation procedures for model selection. Statistics Surveys, 4, 40–79. https://doi.org/10.1214/09-SS054

Bag, R., Mondal, I., Dehbozorgi, M., Bank, S.P., Das, D.N., Bandyopadhyay, J., Pham, Q.B., Al-Quraishi, A.M.F. and Nguyen, X.C., 2022. Modelling and mapping of soil erosion susceptibility using machine learning in a tropical hot sub-humid environment. Journal of Cleaner Production, 364, p.132428. https://doi.org/10.1016/j.jclepro.2022.132428

Bakhtiari, M., Darvishi Boloorani, A., Kakroodi, A.A., Rangzan, K. and Mousivand, A., 2021. Land degradation modeling of dust storm sources using MODIS and meteorological time series data. Journal of Arid Environments, 190, p.104507. https://doi.org/10.1016/j.jaridenv.2021.104507

Berardino, P., Fornaro, G., Lanari, R. and Sansosti, E., 2003. A new algorithm for surface deformation monitoring based on small baseline differential SAR interferograms. IEEE Transactions on Geoscience and Remote Sensing, 40(11), pp.2375-2383. https://doi.org/10.1109/TGRS.2002.803792

Boussalim, Y. and Dallahi, Y., 2026. Integrated RUSLE-machine learning modeling for water erosion risk assessment under climate change in a Mediterranean semi-arid region: a comparison of LR, SVM, and RF models. Arabian Journal of Geosciences, 19(4), p.57. https://doi.org/10.1007/s12517-026-12478-4

Borrelli, P., Robinson, D.A., Fleischer, L.R., Lugato, E., Ballabio, C., Alewell, C., Meusburger, K., Modugno, S., Schütt, B., Ferro, V. and Bagarello, V., 2017. An assessment of the global impact of 21st century land use change on soil erosion. Nature communications, 8(1), p.2013. https://doi.org/10.1038/s41467-017-02142-7

Borrelli, P., Robinson, D.A., Panagos, P., Lugato, E., Yang, J.E., Alewell, C., Wuepper, D., Montanarella, L. and Ballabio, C., 2020. Land use and climate change impacts on global soil erosion by water (2015-2070). Proceedings of the National Academy of Sciences, 117(36), pp.21994-22001. https://doi.org/10.1073/pnas.2001403117

Cerdà, A., Keesstra, S.D., Rodrigo-Comino, J., Novara, A., Pereira, P., Brevik, E., Giménez-Morera, A., Fernández-Raga, M., Pulido, M., Di Prima, S. and Jordán, A., 2017. Runoff initiation, soil detachment and connectivity are enhanced as a consequence of vineyards plantations. Journal of environmental management, 202, pp.268-275. https://doi.org/10.1016/j.jenvman.2017.07.036

Cortes, C. and Vapnik, V., 1995. Support-vector networks. Machine learning, 20(3), pp.273-297. https://doi.org/10.1007/BF00994018

Darvishi Boloorani, A., Bakhtiari, M., Neysani Samany, N., Papi, R., Soleimani, M., Mirzaei, S. and Bahrami, H.A., 2023a. Land degradability mapping using remote sensing data and soil chemical properties. Remote Sensing Applications: Society and Environment, 32, p.101027. https://doi.org/10.1016/j.rsase.2023.101027

Darvishi Boloorani, A., Soleimani, M., Papi, R., Neysani Samany, N., Teymouri, P. and Soleimani, Z., 2023c. Sources, drivers, and impacts of sand and dust storms: a global view. In Dust and health: Challenges and solutions (pp. 31-49). Cham: Springer International Publishing. https://doi.org/10.1007/978-3-031-21209-3_3

Darvishi Boloorani, A., Soleimani, Z., Teymouri, P., Neysani Samany, N., Soleimani, M. and Papi, R., 2023b. Microbiology of sand and dust storms and the effects on human health in Iran and other Persian Gulf countries. In Dust and health: challenges and solutions (pp. 157-186). Cham: Springer International Publishing. https://doi.org/10.1007/978-3-031-21209-3_9

Domazetović, F., Šiljeg, A., Lončar, N. and Marić, I., 2019. Development of automated multicriteria GIS analysis of gully erosion susceptibility. Applied geography, 112, p.102083. https://doi.org/10.1016/j.apgeog.2019.102083

Ebrahimzadeh, S., Soleimani, M., Atarchi, S., Saadat Novin, M. and Shabanian, H., 2023. Detection of areas with severely eroded soils using Sentinel-1 interferometric SAR coherence (Study area: Khuzestan province). Engineering Journal of Geospatial Information Technology, 11(3), pp.59-84. http://dx.doi.org/10.61186/jgit.11.3.59 (Persian).

Esmali Ouri, A., Golshan, M., Janizadeh, S., Cerdà, A. and Melesse, A.M., 2020. Soil erosion susceptibility mapping in Kozetopraghi catchment, Iran: a mixed approach using rainfall simulator and data mining techniques. Land, 9(10), p.368. https://doi.org/10.3390/land9100368

Funk, C., Peterson, P., Landsfeld, M., Pedreros, D., Verdin, J., Shukla, S., Husak, G., Rowland, J., Harrison, L., Hoell, A. and Michaelsen, J., 2015. The climate hazards infrared precipitation with stations—a new environmental record for monitoring extremes. Scientific data, 2(1), p.150066. https://doi.org/10.1038/sdata.2015.66

Goel, A. and Srivastava, S.K., 2016. Role of kernel parameters in performance evaluation of SVM. In 2016 Second international conference on computational intelligence & communication technology (CICT) (pp. 166-169). IEEE. https://doi.org/10.1109/CICT. 2016.40

Haftu, M., Gidey, E., Mhangara, P. and Dikinya, O., 2025. Exploring the relationship between annual soil loss and formation rate in different land use scenarios using support vector machine (SVM) learning models in Tigray Highlands. Scientific Reports, 15(1), p.39146. https://doi.org/10.1038/s41598-025-26881-6

Hanssen, R.F., 2002. Radar system theory and interferometric processing. In: Radar Interferometry. Remote Sensing and Digital Image Processing, vol 2. Springer, Dordrecht. https://doi.org/10.1007/0-306-47633-9_2

Hengl, T., Mendes de Jesus, J., Heuvelink, G.B., Ruiperez Gonzalez, M., Kilibarda, M., Blagotić, A., Shangguan, W., Wright, M.N., Geng, X., Bauer-Marschallinger, B. and Guevara, M.A., 2017. SoilGrids250m: Global gridded soil information based on machine learning. PLoS one, 12(2), p.e0169748. https://doi.org/10.1371/journal.pone.0169748

Hersbach, H., Bell, B., Berrisford, P., Hirahara, S., Horányi, A., Muñoz-Sabater, J., Nicolas, J., Peubey, C., Radu, R., Schepers, D. and Simmons, A., 2020. The ERA5 global reanalysis. Quarterly journal of the Royal Meteorological Society, 146(730), pp.1999-2049. https://doi.org/10.1002/qj.3803

Huang, Y. and Zhao, L., 2018. Review on landslide susceptibility mapping using support vector machines. Catena, 165, pp.520-529. https://doi.org/10.1016/j.catena.2018.03.003

Jensen, J. R., 1996. Introductory Digital Image Processing: A Remote Sensing Perspective (2nd ed.). Upper Saddle River, NJ, USA: Prentice Hall. ISBN: 9780132058407.

Kandel, D.D., Western, A.W. and Grayson, R.B., 2005. Scaling from process timescales to daily time steps: A distribution function approach. Water Resources Research, 41(2). https://doi.org/10.1029/2004WR003380

Kavzoglu, T., Sahin, E.K. and Colkesen, I., 2014. Landslide susceptibility mapping using GIS-based multi-criteria decision analysis, support vector machines, and logistic regression. Landslides, 11(3), pp.425-439. https://doi.org/10.1007/s10346-013-0391-7

Khalil, R.Z., 2018. InSAR coherence-based land cover classification of Okara, Pakistan. The Egyptian Journal of Remote Sensing and Space Science, 21, pp.S23-S28. https://doi.org/10.1016/j.ejrs.2017.08.005

Khodadadi, M., Mabit, L., Zaman, M., Porto, P. and Gorji, M., 2019. Using 137Cs and 210Pbex measurements to explore the effectiveness of soil conservation measures in semi-arid lands: a case study in the Kouhin region of Iran. Journal of Soils and Sediments, 19(4), pp.2103-2113. https://doi.org/10.1007/s11368-018-2205-y

Kim, J., Dorjsuren, M., Choi, Y. and Purevjav, G., 2020. Reconstructed aeolian surface erosion in southern Mongolia by multi-temporal InSAR phase coherence analyses. Frontiers in Earth Science, 8, p.531104. https://doi.org/10.3389/feart.2020.531104

Lal, R., 2001. Soil degradation by erosion. Land degradation & development, 12(6), 519-539. https://doi.org/10.1002/ldr.472

Lal, R., 2003. Soil erosion and the global carbon budget. Environment international, 29(4), 437-450. https://doi.org/10.1016/S0160-4120(02)00192-7

Lei, X., Chen, W., Avand, M., Janizadeh, S., Kariminejad, N., Shahabi, H., Costache, R., Shahabi, H., Shirzadi, A. and Mosavi, A., 2020. GIS-based machine learning algorithms for gully erosion susceptibility mapping in a semi-arid region of Iran. Remote Sensing, 12(15), p.2478. https://doi.org/10.3390/ rs12152478

Liu, J.G., Lee, H. and Pearson, T., 1999, December. Detection of rapid erosion in SE Spain using ERS SAR interferometric coherence imagery. In Remote Sensing for Earth Science, Ocean, and Sea Ice Applications (Vol. 3868, pp. 525-535). SPIE. https://doi.org/10.1117/12.373131

Maxwell, A.E., Warner, T.A. and Fang, F., 2018. Implementation of machine-learning classification in remote sensing: An applied review. International journal of remote sensing, 39(9), pp.2784-2817. https://doi.org/10.1080/01431161.2018.1433343

Mohebzadeh, H., Biswas, A., Rudra, R. and Daggupati, P., 2022. Machine learning techniques for gully erosion susceptibility mapping: a review. Geosciences, 12(12), p.429. https://doi.org/10.3390/geosciences12120429

Mountrakis, G., Im, J. and Ogole, C., 2011. Support vector machines in remote sensing: A review. ISPRS Journal of Photogrammetry and Remote Sensing, 66(3), pp.247-259. https://doi.org/10.1016/j.isprsjprs.2010.11.001

Muratoreanu, G., Dunea, D., Tanislav, D., Reid, M., Diaconu, D.C., Costache, A., Serban, G., Pastor, I. and Bretcan, P., 2025. Soil erosion susceptibility assessment in the Bistrița River basin (Romania) using machine learning algorithms and GIS. Scientific Reports, 15(1), p.44381. https://doi.org/10.1038/s41598-025-28184-2

Mosavi, A., Sajedi-Hosseini, F., Choubin, B., Taromideh, F., Rahi, G. and Dineva, A.A., 2020. Susceptibility mapping of soil water erosion using machine learning models. Water, 12(7), p.1995. https://doi.org/10.3390/w12071995

Pal, M. and Mather, P.M., 2005. Support vector machines for classification in remote sensing. International journal of remote sensing, 26(5), pp.1007-1011. https://doi.org/10.1080/01431160512331314083

Panagos, P., Borrelli, P., Poesen, J., Ballabio, C., Lugato, E., Meusburger, K., Montanarella, L. and Alewell, C., 2015. The new assessment of soil loss by water erosion in Europe. Environmental science & policy, 54, pp.438-447. https://doi.org/10.1016/j.envsci.2015.08.012

Papi, R., Attarchi, S., Soleimani, M., 2020. Analysing Time Series of Land Subsidence in the West of Tehran Province (Shahriar Plain) and its Relation to Groundwater Discharge by InSAR Technique, Geography and Environmental Sustainability, 10(1), pp. 109-128. https://doi.org/10.22126/ges.2020.4933.2182 (Persian).

Rahmati, O., Kornejady, A., Samadi, M., Deo, R.C., Conoscenti, C., Lombardo, L., Dayal, K., Taghizadeh-Mehrjardi, R., Pourghasemi, H.R., Kumar, S. and Bui, D.T., 2019. PMT: New analytical framework for automated evaluation of geo-environmental modelling approaches. Science of the total environment, 664, pp.296-311. https://doi.org/10.1016/j.scitotenv.2019.02.017

Ren, F., Li, Y. and Hu, M., 2018. Multi-classifier ensemble based on dynamic weights. Multimedia Tools and Applications, 77(16), pp.21083-21107. https://doi.org/10.1007/s11042-017-5480-5

Rodriguez, E., Morris, C.S. and Belz, J.E., 2006. A global assessment of the SRTM performance. Photogrammetric Engineering & Remote Sensing, 72(3), pp.249-260. https://doi.org/10.14358/PERS.72.3.249

Saha, S., Roy, J., Arabameri, A., Blaschke, T. and Tien Bui, D., 2020. Machine learning-based gully erosion susceptibility mapping: A case study of Eastern India. Sensors, 20(5), p.1313. https://doi.org/10.3390/s20051313

Sarkar, T. and Mishra, M., 2018. Soil erosion susceptibility mapping with the application of logistic regression and artificial neural network. Journal of Geovisualization and

Spatial Analysis, 2(1), p.8. https://doi.org/10.1007/s41651-018-0015-9

Syarif, I., Prugel-Bennett, A. and Wills, G., 2016. SVM parameter optimization using grid search and genetic algorithm to improve classification performance. TELKOMNIKA (Telecommunication Computing Electronics and Control), 14(4), pp.1502-1509. http://doi.org/10.12928/telkomnika.v14i4.3956

Senanayake, S., Pradhan, B., Huete, A. and Brennan, J., 2020. A review on assessing and mapping soil erosion hazard using geo-informatics technology for farming system management. Remote sensing, 12(24), p.4063. https://doi.org/10.3390/rs12244063

Sharifikia, M. and Rabbani, F., 2020. Source routing and detection of dust storm in the Salt Lake basin of Qom in Iran. Arabian Journal of Geosciences, 13(14), p.678. https://doi.org/10.1007/s12517-020-05596-0

Simons, M. and Rosen, P.A., 2007. Interferometric synthetic aperture radar geodesy. In Treatise on geophysics (pp. 391-446). https://doi.org/10.1016/B978-044452748-6.00059-6

Soleimani, M., Attarchi, S., Mahmoody-Vanolya, N., Bakhshizadeh, F. and Ahmadi, H., 2021. Evaluation of Sentinel-1 Interferometric SAR Coherence efficiency for Land Cover Mapping. Engineering Journal of Geospatial Information Technology, 9(3), pp.85-107. http://dx.doi.org/10.52547/jgit.9.3.85 (Persian).

Smola, A.J. and Schölkopf, B., 2004. A tutorial on support vector regression. Statistics and computing, 14(3), pp.199-222. https://doi.org/10.1023/B:STCO.0000035301.49549.88

Touzi, R., Lopes, A., Bruniquel, J. and Vachon, P.W., 2002. Coherence estimation for SAR imagery. IEEE transactions on geoscience and remote sensing, 37(1), pp.135-149. https://doi.org/ 10.1109/36.739146

Vapnik, V., 2013. The nature of statistical learning theory. Springer science & business media. https://doi.org/10.1007/978-1-4757-2440-0

Xuedong, Z., Wenxi, L. and Shuguang, H., 2018. Urban Change Detection in TerraSAR Image Using the Difference Method and SAR Coherence Coefficient. Journal of Engineering Science & Technology Review, 11(3). https://doi.org/10.25103/jestr.113.03

Žížala, D., Juřicová, A., Zádorová, T., Zelenková, K. and Minařík, R., 2019. Mapping soil degradation using remote sensing data and ancillary data: South-East Moravia, Czech Republic. European Journal of Remote Sensing, 52(sup1), pp.108-122. https://doi.org/10.1080/22797254.2018.1482524